2023 IEEE International Conference on Robotics and Automation (ICRA 2023)
May 29 - June 2, 2023. London, UK

Concept Design of a New XY Compliant Parallel Manipulator With Spatial Configuration

Zekui Lyu and Qingsong Xu, *Senior Member, IEEE*

***Abstract*— This paper proposes the concept design of a novel XY compliant parallel manipulator (CPM) with spatial configuration, which is beneficial to promote the performance of the XY CPM. Evolved from a planar configuration, a spatial compliant parallelogram flexure is devised as the basic module structure. Then, a mirror-symmetric XY CPM adopting spatial layout is proposed based on four-prismatic-prismatic (4-PP) parallel mechanism. The prototypes are fabricated by 3D printing for testing. The performance analysis and verification is conducted through theoretical modeling, finite element simulation, and experimental study. For comparison study, a planar XY CPM with similar mechanism is also developed. Results show that the proposed XY CPM with spatial configuration provides the benefits of smaller plane footprint, large working stroke, and enhanced load-bearing capacity as compared to the planar one. It is appropriate for precise positioning scenarios, like soft-contact lithography, which require high loading capacity and great compactness.**

I. Introduction

The XY compliant parallel manipulator (CPM) is a crucial component of various precision equipment, which can realize functions such as step positioning, path scanning, and trajectory tracking in a plane. It has been employed in a variety of applications, e.g., nanolithography, atomic force microscopes, bio-manipulation, and semiconductor inspection [1], [2]. Thanks to the superior characteristics of compliant hinges and parallel mechanisms, the XY CPM can deliver accurate and reliable 2D planar motion [3]–[5].

The traditional design of XY CPM gives more consideration to the selection and arrangement of the compliant hinges on a plane to achieve the desired performance. Such design results in a planar configuration, as the mechanism's horizontal dimensions are greater than its vertical height. Piezoelectric actuator (PZT) is a typical driving source for the CPM, and its issue of limited output stroke can be alleviated by using displacement amplification mechanism [6], [7]. However, it is difficult to achieve a centimeter-level travel range with PZT actuator [8]. To realize larger motion stroke, several XY CPMs utilizing voice coil motors (VCM) and leaf flexures were developed in the literature [9]–[11]. To prolong the stage's stroke up to millimeter or even centimeter level, researchers have constructed mirror-symmetric mechanisms based on compound parallelogram flexure (CPF) and multistage CPF [10]. However, there are still limitations in optimizing the performance of CPM by structural design based on a planar configuration.

In particular, the design of XY CPM with planar configuration faces two challenging issues. On the one hand, the driving stiffness of the mechanism requires to be lessened to broaden the manipulator's travel stroke. Increasing the length of the compliant hinge is an effective method, but it comes with a bulky size. On the other hand, the out-of-plane stiffness should be greater to raise its load-bearing capacity. Thickening the compliant hinge can strengthen the vertical stiffness, however, it will lead to a growth in the actuation stiffness. These contradictions may be solved by introducing a vertical spatial architecture. For example, to reduce the driving stiffness, Xu and Roy et al. stacked the same or identical components in vertical direction of XY CPMs, which significantly diminished the plane footprint of the CPMs [12], [13]. The stacking mechanism utilizes the concept of modular design to minimize the horizontal area occupancy and makes it easy to repair and reassemble. To strengthen the mechanism's load-bearing capacity, Shang and Cai et al. installed four supporting legs with hook hinges underneath the intermediate platform [14], [15]. In view of the physical size of the VCM, there is an empty vertical space beneath the central platform itself. Hence, these supports do not vastly increase the CPM's height. Moreover, XY CPMs have many other complicated spatial configurations, such as vertically placing parallelogram flexure, hybrid mechanism by combining serial and parallel connections, position space-based reconfiguration method, and so on [16]–[20]. However, these XY CPMs with spatial configuration also suffer from manufacturing difficulties, assembly errors, and complex actuator settings. In addition, previous work does not consider the mutual conversion and comparison between planar and spatial configurations.

To this end, this paper introduces a novel XY CPM with spatial configuration, which is evolved from a traditional planar mechanism. Fig. 1 depicts how the two conceptual designs are transformed. Without compromising motion travel range, the spatial CPM can drastically reduce the plane footprint of the mechanism. Hence, it is a compact device which can be adapted to space-constrained application scenarios. The load-carrying capacity of the CPM has been significantly increased as a result of spatial mirror-symmetric design. In addition, the assembly-free monolithic design of the CPM mechanism is compatible with 3D printing fabrica-

This work was supported in part by the National Natural Science Foundation of China under Grant 52175556, the Macao Science and Technology Development Fund under Grant 0022/2019/AKP, 0153/2019/A3 and 0102/2022/A2, and Research Committee of the University of Macau under Grant MYRG2022-00068-FST and MYRG-CRG2022-00004-FST.

The authors are with the Department of Electromechanical Engineering, Faculty of Science and Technology, University of Macau, Macau, China.

Corresponding author: Q. Xu (phone: +853-88224278; fax: +853-88222426; e-mail: qsxu@umac.mo).

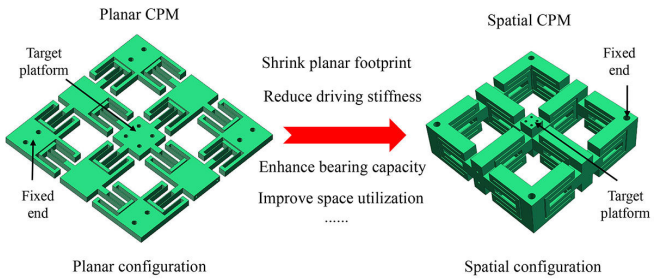

Fig. 1. The mechanism layout of an XY CPM from planar to spatial configuration.

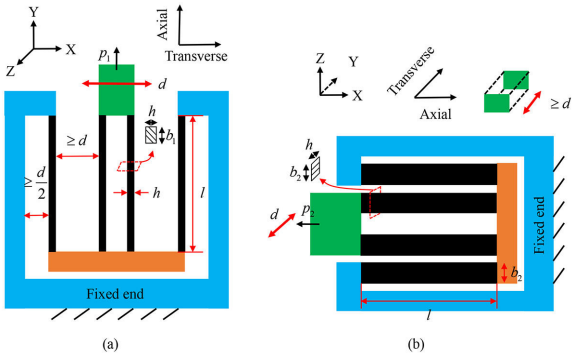

Fig. 2. Illustration of planar and spatial CPFs with geometrical parameters: (a) Planar CPF; (b) spatial CPF.

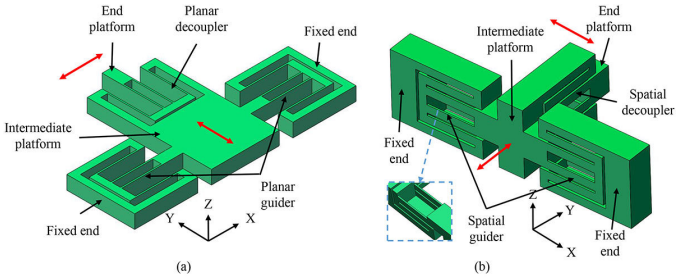

Fig. 3. Illustration of planar and spatial PP joints: (a) Planar PP joint; (b) spatial PP joint.

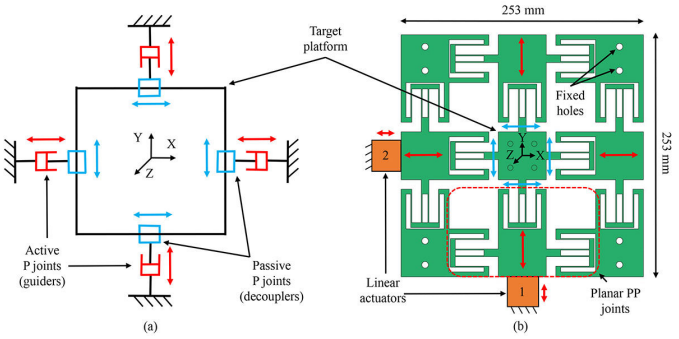

Fig. 4. 4-PP layout and its planar realization: (a) 4-PP layout; (b) planar CPM.

tion method. Its superior performance has been confirmed by simulation study and experimental test. The reported concept design ranging from planar to spacial configuration will provide a new idea or reference to develop high-performance CPM.

II. Concept Design from Planar to Spatial Configuration

Due to its large motion stroke and small parasitic displacement, CPF has been widely used as prismatic (P) joint. A typical CPF with geometric parameters in XY plane arrangement is shown in Fig. 2(a). Its terminal (green block) can realize the motion transmission in X-axis direction. This motion transmission is primarily obtained by the deformation of the middle four leaf flexures (black bar). The CPF in such configuration has a significant length in both X- and Y-axes. The longer dimension in Y-axis direction realizes a lower stiffness of the leaf flexure. As indicated in Fig. 2(a), specific constraints are required for the mechanism to prevent a collision between the flexible parts and rigid-bodies of the mechanism, which leads to the extension of the mechanism size in X-axis direction. As illustrated in Fig. 2(b), a novel CPF with vertical plane arrangement has been devised to shrink the size of the CPF in the horizontal plane. It approximately transfers the length occupation of the original CPF in Y-axis to that in Z-axis. Its terminal can realize linear motion parallel to the Y-axis, which is perpendicular to XZ plane where the mechanism is located. The clearance setting of the mechanism in Y-axis direction should be larger than the maximum movable distance (d) to prevent limited contact, and this required clearance is about $3d$ in the original design. Hence, the horizontal area occupancy is reduced by adopting the new CPF as basic module.

Based on the aforementioned CPF, a planar and a spatial PP joints are introduced as illustrated in Fig. 3. The compliant PP joint is generally devised to kinematically decouple the mechanism motion in two orthogonal directions. The planar PP joint is composed of three CPFs, with the first two (guider) connected in parallel to transmit motion in Y-axis and the third CPF (decoupler) connected in series with an intermediate platform to withstand the deformation in X-axis. Similarly, the spatial PP joint is also made of a set of spatial guiders and a spatial decoupler linked in series. The difference lies in that the spatial PP joint contains six spatial CPFs. That is, each previous planar CPF is replaced with two parallel spatial CPFs, which are separated by sufficient distance to prevent motion conflicts. Meanwhile, the width of leaf flexure in spatial CPF is shorter than that in planar CPF. The reason lies in that the mechanism made of spatial CPF does not have this weakness naturally, whereas the mechanism made of planar CPF has to increase the thickness to better suppress vertical vibration modes.

Afterward, the conceptual design of an XY CPM based on 4-PP mechanism is presented. The 4-PP layout has a stricter symmetry than the 2-PP design, which can further eliminate unfavorable behaviors, such as cross-coupling motion and in-plane rotation, as shown in Fig. 4(a). For comparison study, a planar 4-PP CPM based on the designed planar PP joint is adopted as shown in Fig. 4(b). Under the driving of linear

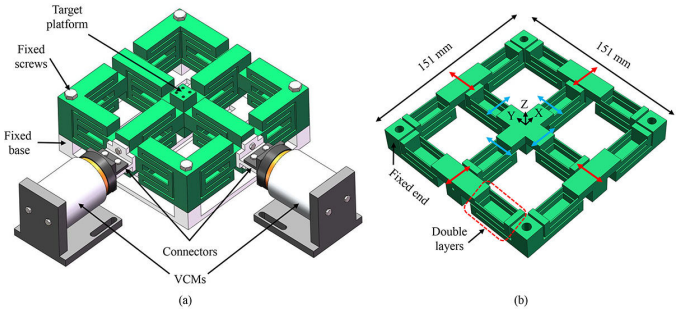

Fig. 5. The spatial configuration of CPM :(a) The purposed spatial CPM with the 4-PP layout; (b) its cross-sectional view at half height.

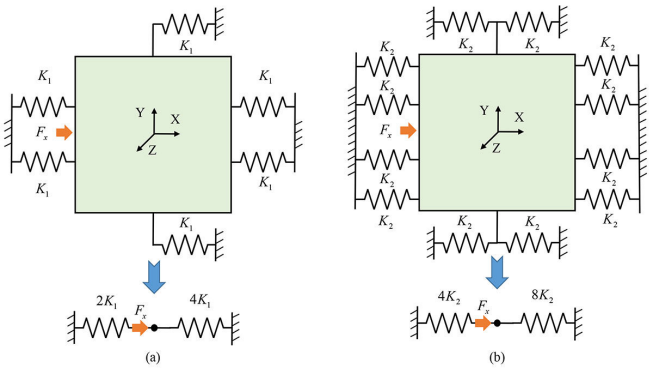

Fig. 6. Stiffness model: (a) Planar CPM; (b) spatial CPM.

actuators on both sides, the target platform enables a large-stroke orthogonal decoupling motion. Due to the configuration of multiple sets of CPFs, the planar CPM has a larger plane area. The CPM is required to have a compact plane footprint to make the device more sophisticated for many application scenarios, including soft-contact lithography and electron beam lithography [21].

To this end, a novel spatial 4-PP CPM with two VCMs is proposed as shown in Fig. 5. It not only allows a large-stroke motion transmission, but also guarantees a limited plane occupancy. This is enabled by the fundamental elements (e.g., spatial PP joints and spatial CPFs) which comprise the spatial CPM by adapting the physical dimensions in vertical direction. Moreover, its spatial arrangement also considerably increases the load-carrying capacity of the output platform. Fig. 5(b) provides a cross-sectional view of the proposed spacial CPM in the horizontal plane at half height. It is observed that the original planar CPF has been replaced with a double-layer guiding mechanism, which is made of two spatial CPFs with a certain distance. Although the output platform in the spatial CPM has a smaller area than the planar design does, many applications can be satisfied by mounting an extra top stage.

III. Stiffness Analysis and Finite-Element Simulation Study

A. Stiffness Analysis and Dimension Comparision

The analysis of the driving stiffness for the proposed planar and spatial CPMs is conducted in this section. As shown in Fig. 2, the stiffnesses of the planar CPF (K_{p-cpf}) and spatial CPF (K_{s-cpf}) can be derived below.

$$K_{p-cpf} = 12\frac{EI_1}{l^3} - 0.03\frac{p_1^2 l}{EI_1} \tag{1}$$

$$K_{s-cpf} = 12\frac{EI_2}{l^3} - 0.03\frac{p_2^2 l}{EI_2} \tag{2}$$

where E denotes Young's modulus of the material, and l is the length of all leaf flexures [22]. I_1 and I_2 are the moments of inertia of the cross-section with $I_1 = \frac{b_1 h^3}{12}$ and $I_2 = \frac{b_2 h^3}{12}$, where h is the width of all leaf flexures, b_1 is the thickness of the planar leaf flexures, and b_2 is the thickness (along Z-axis) of the spatial leaf flexures. In addition, p_1 and p_2 represent the axial forces subjected by the end of the planar CPF and spatial CPF, respectively. Here, only the bending deformation of leaf flexures is taken into account for simplicity. The stiffness models of the proposed planar CPM and spatial CPM in one direction are shown in Fig. 6(a) and (b), respectively. The basic CPF is treated as a spring in this stiffness model, and the whole model is derived in accordance with their serial or parallel connection. According to the aforementioned formulas, $K_1 = 12\frac{EI_1}{l^3}$ and $K_2 = 12\frac{EI_2}{l^3}$ can be obtained by referring to Fig. 6(a) and (b), respectively. Furthermore, the stiffnesses of the planar CPM (K_p) and spatial CPM (K_s) can be derived as follows.

TABLE I
Dimensions of the Proposed Planar and Spatial CPMs

Type	Dimension of leaf flexure	Dimension of CPM
Planar	$30 \times 10 \times 1$ (mm^3)	$253 \times 253 \times 10$ (mm^3)
Spatial	$30 \times 5 \times 1$ (mm^3)	$151 \times 151 \times 42$ (mm^3)

$$K_p \approx 6K_1 = 72\frac{EI_1}{l^3} \tag{3}$$

$$K_s \approx 12K_2 = 144\frac{EI_2}{l^3} \tag{4}$$

The dimensions of the planar and spatial CPMs are given in Table I, including the sizes of leaf flexures and the whole mechanism (without actuators). To compare the performances of the planar and spatial designs, an approximative mechanical structure was applied to the two layouts. It is found that the spatial CPM's plane area is only 35.62% that of the planar one, indicating that the spatial design is more compact in horizontal plane. This is contributed by the spatial layout which smartly exploits the spare vertical space. From the perspective of mechanism, the vertical dimension of the spatial CPM is much larger than that of the planar one. In consideration of the height (e.g., 46 mm) of the VCM actuator, the vertical dimension of the spatial CPM is close to that of the planar one.

B. FEA Simulation

The performances of the two CPMs are evaluated through FEA simulation study. The material is selected as common

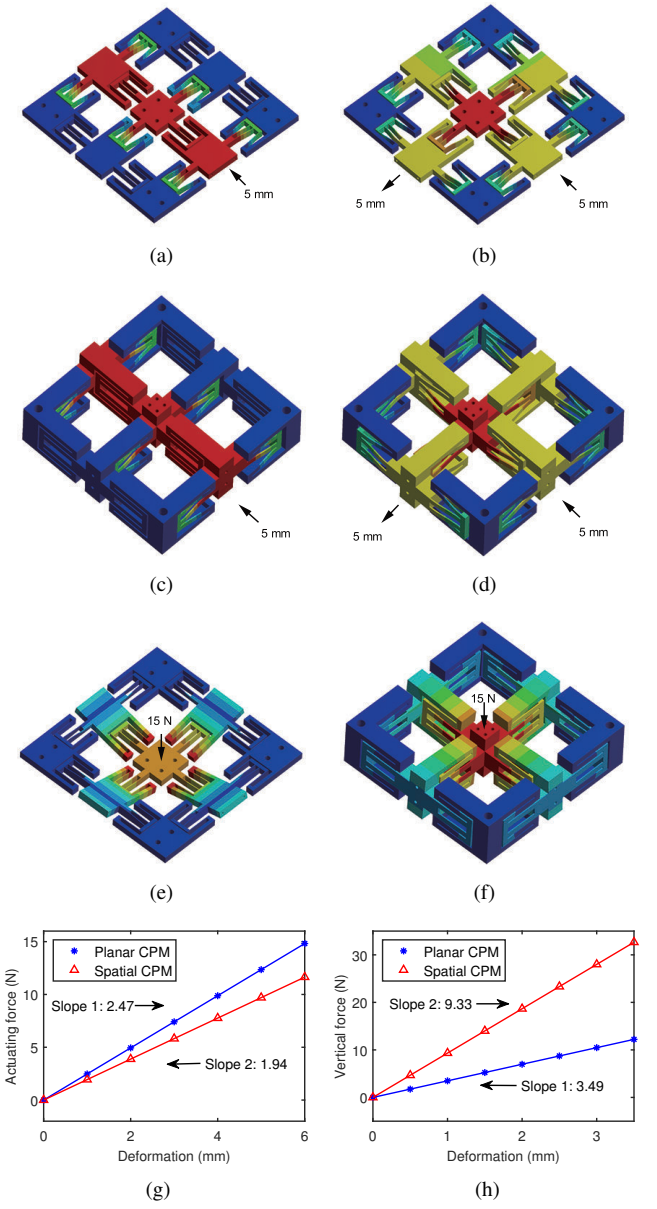

Fig. 7. Simulation results. (a) Planar CPM with one axis actuating; (b) planar CPM with two axes actuating; (c) spatial CPM with one axis actuating; (d) spatial CPM with two axes actuating; (e) planar CPM with vertical loading; (f) spatial CPM with vertical loading; (g) driving stiffness of the two CPMs; (h) vertical stiffness of the two CPMs.

resin with high strength and high toughness. In the simulation, the standard earth gravity and large deflection are activated to enhance the simulation accuracy.

By assigning a linearly variable displacement to the actuating end and monitoring its reaction force, the driving stiffness of the CPM is determined. When an input displacement of 5 mm is acted on the planar and spatial CPMs, their deformation shapes are shown in Fig. 7(a) and (c), respectively. The linear fitting results of the stiffness simulations are presented in Fig. 7(g). The planar and spatial CPMs have similar actuation stiffnesses, i.e., 2.47 N/mm and 1.94 N/mm, respectively. Since the latter one is slightly smaller than the

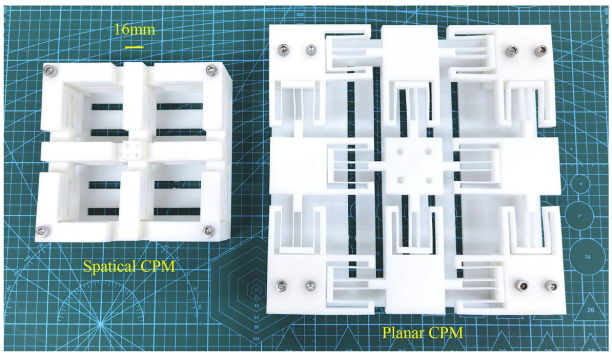

Fig. 8. Prototypes of fabricated planar and spatial CPMs by 3D printing.

former one, the spatial CPM can provide larger working stroke under the same driving force. For both mechanisms, a stroke of centimeter range is desired. The two actuating ends of the mechanism are each moved by 5 mm, and Fig. 7(b) and (d) depict the deformation results. The output platforms of both manipulators are capable of large decoupling motion without material yield.

A similar approach is taken to assess the out-of-plane stiffness of the output platform in vertical direction. Fig. 7(e) and (f) display the deformation results of the two mechanisms under a vertical force of 15 N. Fig. 7(h) depicts the results of vertical stiffness. It is seen that the load-bearing stiffness of the spatial CPM (9.33 N/mm) is greater than that of the planar CPM (3.49 N/mm). This is attributed to the reinforced configuration of the spatial CPM. Meanwhile, the safety factor (9.71) of the spatial CPM is larger than that of the planar CPM (7.85), indicating that the load-bearing capacity of the spatial CPM is stronger than the planar one.

IV. Experiment Testing Results

A. Prototype Fabrication and Tests

The prototypes of the two CPMs have been fabricated by using 3D printing (additive manufacturing) technology with the material of white common resin. As shown in Fig. 8, a more compact plane occupation of the proposed spatial CPM can be observed. Due to the mirror symmetry of the designed mechanism, the following verification experiments are conducted in one motion axis.

First, the driving stiffness and vertical passive stiffness of the two CPMs have been tested. The related equipment are shown in Fig. 9(a) and (b). By pushing the CPM through an XYZ micropositioner (model: Z285, from Thorlabs Inc.) equipped with force sensors (model: LSB200, from FUTEK Advanced Sensor Technology, Inc.) and monitoring the deformation with a laser displacement sensor (model: LK-H055, from Keyence Corp.), the driving stiffness of the mechanism is acquired. As shown in Fig. 9(c) and (d), the driving stiffnesses of the planar and spatial CPMs are determined as 1.85 N/mm and 1.72 N/mm, respectively. The two values are close to each other due to similar dimension design of the compliant hinges. The vertical stiffness is measured in a similar manner, except that the actuation force

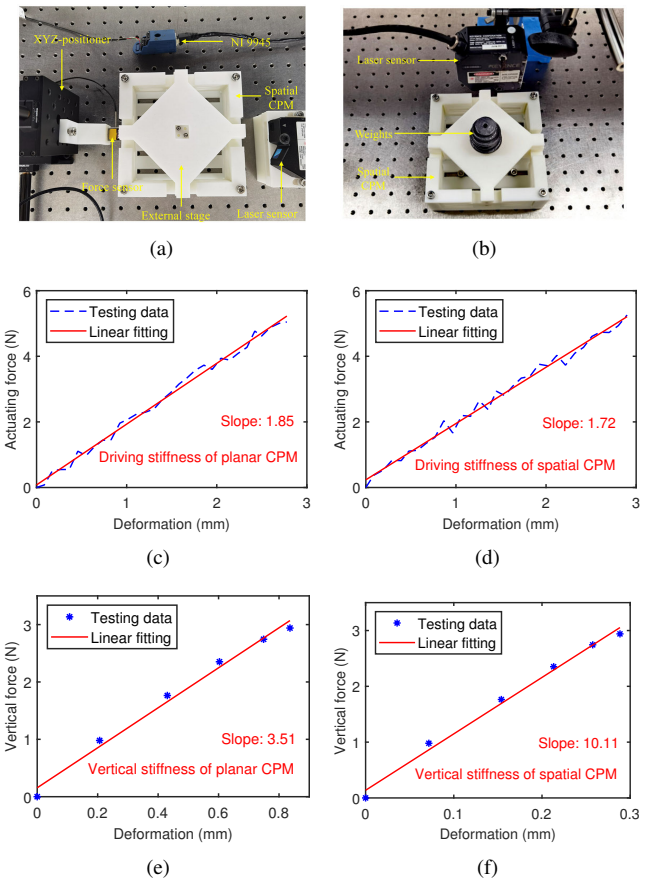

Fig. 9. Testing of driving stiffness and vertical stiffness: (a) Driving stiffness testing equipment; (b) vertical stiffness testing equipment; (c) driving stiffness of planar CPM; (d) driving stiffness of spatial CPM; (e) vertical stiffness of planar CPM; and (f) vertical stiffness of spatial CPM.

is provided by the gravity of different weights. As shown in Fig. 9(e) and (f), the measured vertical stiffness of the two CPMs are 3.51 N/mm and 10.11 N/mm, respectively. The vertical stiffness of the spatial one is approximately 3 times that of the planar one, indicating that the spatial CPM has a greater load-carrying capacity without material yield.

Second, the working strokes of the two CPMs were obtained by using the experimental setup as shown in Fig. 10(a). The motion of the output platform is produced by two VCMs (model: NCC05-18-060-2X, from H2W Techniques, Inc.), and the displacement is measured by two laser displacement sensors with orthogonal arrangement. A real-time controller (NI cRIO-9022 controller, from National Instruments Inc.) is adopted to produce the driving signals with voltage output module (NI-9263 board) and acquire the sensor signals with analog input module (NI-9015 board). Specifically, a sinusoidal voltage signal with a frequency of 0.5 Hz and an amplitude of 3 V is applied to drive the VCM, and the measured output displacements of the planar and spatial CPMs are shown in Fig. 10(b) and (c), respectively. It is observed that the motion strokes of the planar and spatial CPMs are 10.17 mm and 10.29 mm, respectively. The gaps in the forward and backward motion travels is induced by

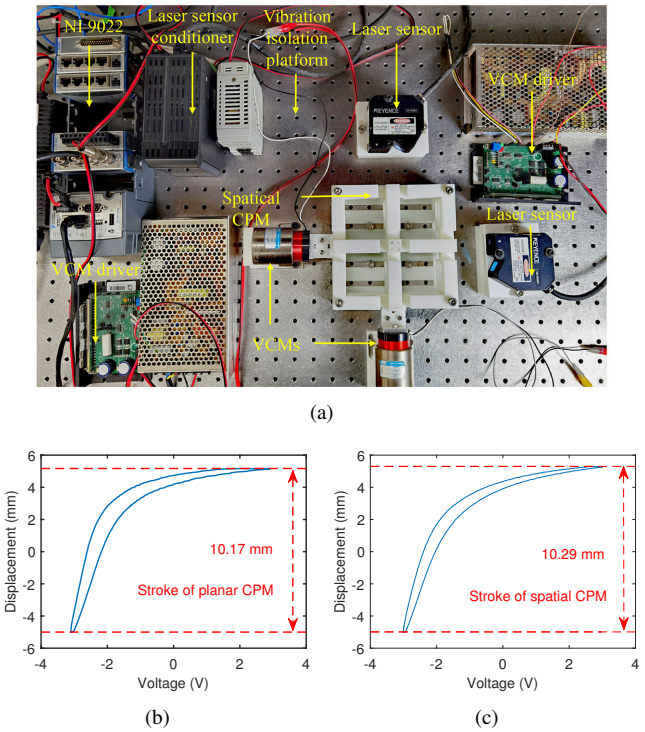

Fig. 10. Testing of working stroke: (a) working stroke testing equipment; (b) stroke of planar CPM; (c) stroke of spatial CPM.

TABLE II
COMPARISON OF THEORETICAL MODEL, SIMULATION, AND EXPERIMENTAL RESULTS

Method	Driving stiffness (N/mm)		Vertical stiffness (N/mm)	
	Planar	Spatial	Planar	Spatial
Theoretical model	1.96	1.96	-	-
Simulation	2.47	1.94	3.49	9.33
Experimental results	1.85	1.72	3.51	10.11

the hysteresis of the electromagnetic actuators and materials, which can be lessened by using closed-loop control. The two mechanisms can generate a centimeter-level stroke without damage, demonstrating their superior motion transmission performance.

B. Performance Comparison and Discussion

The driving stiffness and vertical passive stiffness of the two mechanisms obtained by the theoretical model, simulation, and experimental tests are compared in Table II. The results demonstrate good consistency. As compared with modeling result, the slightly lower experimental result of the driving stiffness is mainly caused by manufacturing errors and measurement errors. Due to the material's characteristics, there is a fast and large displacement response once the weight is placed on the output platform, followed by a slow and minor drop of the displacement response. Here, only the displacement after fast deformation is adopted for the convenience of testing. It is observed that the experimental result of vertical stiffness is slightly larger than that of simulation result.

TABLE III

PERFORMANCE COMPARISON OF PLANAR AND SPATIAL CPMS

Parameters	Planar CPM	Spatial CPM
Driving stiffness (N/mm)	1.85	1.72
Vertical stiffness (N/mm)	3.49	10.11
Stroke (mm × mm)	10.17×10.17	10.29×10.29
Planar footprint (mm × mm)	253×253	151×151
Area efficiency (%)	0.16	0.46

Table III compares the performances of the two mechanisms, including the planar footprint, stiffness, travel range, and compactness. The compactness of the mechanism is expressed by the area efficiency, which is given below.

$$\text{Area efficiency} = \frac{\text{Stroke}}{\text{Planar footprint}} \tag{5}$$

The above criterion has been used to evaluate the performance of CPM in many works [10], [23], [24]. The low driving stiffness of the spatial CPM ensures its large working stroke under the same actuating force. Due to its reasonable utilization of vertical space, the spatial CPM has a smaller plane footprint. Hence, the spatial CPM has an area efficiency which is nearly 2.87 times better than the planar CPM. In addition, the spatial CPM outperforms the planar one in terms of vertical stiffness (2.90 times) and load-carrying capacity. These advances demonstrate the necessity and significance of the proposed XY CPM with spatial configuration.

V. CONCLUSION

To overcome the shortcomings of conventional XY CPM based on planar configuration design, this paper presents a new spatial design to enhance its compactness and load-bearing capacity. The design process is evolved from planar to spatial configuration. The stiffness modeling and finite element analysis were performed to evaluate the performance of the reported mechanism. Then, the proposed mechanism was fabricated by 3D printing. The driving stiffness, vertical stiffness, and working stroke of the developed XY CPM in both planar and spatial configurations were tested. The results of theoretical model, simulation analysis, and experimental study are in good agreement. Compared to the planar CPM, the proposed spatial CPM has improved the compactness and out-of-plane stiffness by 2.87 times and 2.90 times, respectively. The spatial CPM offers benefits in terms of large working stroke and load-bearing capacity. The proposed spatial XY CPM is desirable for the application circumstances where the operation space is limited.

REFERENCES

[1] M. Rana, H. R. Pota, and I. R. Petersen, "Improvement in the imaging performance of atomic force microscopy: A survey," *IEEE Transactions on Automation Science and Engineering*, vol. 14, no. 2, pp. 1265–1285, 2016.

[2] Q. Xu, *Micromachines for Biological Micromanipulation*. Springer, 2018.

[3] A. Al-Jodah, B. Shirinzadeh, M. Ghafarian, T. K. Das, and J. Pinskier, "Design, modeling, and control of a large range 3-DOF micropositioning stage," *Mechanism and Machine Theory*, vol. 156, p. 104159, 2021.

[4] Q. Xu, *Design and Implementation of Large-Range Compliant Micropositioning Systems*. John Wiley & Sons, 2016.

[5] Z. Lyu and Q. Xu, "Novel design of a piezoelectrically actuated compliant microgripper with high area-usage efficiency," *Precision Engineering*, vol. 76, pp. 1–11, 2022.

[6] Y. K. Yong, S. S. Aphale, and S. R. Moheimani, "Design, identification, and control of a flexure-based XY stage for fast nanoscale positioning," *IEEE Transactions on Nanotechnology*, vol. 8, no. 1, pp. 46–54, 2008.

[7] K.-B. Choi, J. Lee, G. Kim, H. Lim, S. Kwon, and S.-C. Lee, "Design and analysis of a flexure-based parallel XY stage driven by differential piezo forces," *International Journal of Precision Engineering and Manufacturing*, vol. 21, no. 8, pp. 1547–1561, 2020.

[8] F. Wang, X. Zhao, Z. Huo, B. Shi, C. Liang, Y. Tian, and D. Zhang, "A 2-DOF nano-positioning scanner with novel compound decoupling-guiding mechanism," *Mechanism and Machine Theory*, vol. 155, p. 104066, 2021.

[9] S. Awtar and G. Parmar, "Design of a large range XY nanopositioning system," *Journal of Mechanisms and Robotics*, vol. 5, no. 2, p. 021008, 2013.

[10] Q. Xu, "New flexure parallel-kinematic micropositioning system with large workspace," *IEEE Transactions on Robotics*, vol. 28, no. 2, pp. 478–491, 2011.

[11] Y. Liu and Z. Zhang, "A large range compliant XY nano-manipulator with active parasitic rotation rejection," *Precision Engineering*, vol. 72, pp. 640–652, 2021.

[12] Q. Xu, "Design and development of a compact flexure-based XY precision positioning system with centimeter range," *IEEE Transactions on Industrial Electronics*, vol. 61, no. 2, pp. 893–903, 2013.

[13] N. K. Roy and M. A. Cullinan, "Design and characterization of a two-axis, flexure-based nanopositioning stage with 50 mm travel and reduced higher order modes," *Precision Engineering*, vol. 53, pp. 236–247, 2018.

[14] J. Shang, Y. Tian, Z. Li, F. Wang, and K. Cai, "A novel voice coil motor-driven compliant micropositioning stage based on flexure mechanism," *Review of Scientific Instruments*, vol. 86, no. 9, p. 095001, 2015.

[15] K. Cai, Y. Tian, X. Liu, D. Zhang, J. Shang, and B. Shirinzadeh, "Development and control methodologies for 2-DOF micro/nano positioning stage with high out-of-plane payload capacity," *Robotics and Computer-Integrated Manufacturing*, vol. 56, pp. 95–105, 2019.

[16] Z. Liu, Z. Zhang, and P. Yan, "A spatial design of a large stroke compliant XY nanomanipulator with cross-coupling error reduction," in *Proc. of 2019 International Conference on Manipulation, Automation and Robotics at Small Scales (MARSS)*, pp. 1–6, 2019.

[17] S. Fan, H. Liu, and D. Fan, "Design and development of a novel monolithic compliant XY stage with centimeter travel range and high payload capacity," *Mechanical Sciences*, vol. 9, no. 1, pp. 161–176, 2018.

[18] J. Zhu, G. Hao, S. Li, and X. Kong, "A compact mirror-symmetrical XY compliant parallel manipulator for minimizing parasitic rotations," *Journal of Mechanical Design*, vol. 144, no. 7, p. 073303, 2022.

[19] J. Yu, Y. Xie, Z. Li, and G. Hao, "Design and experimental testing of an improved large-range decoupled XY compliant parallel micromanipulator," *Journal of Mechanisms and Robotics*, vol. 7, no. 4, p. 044503, 2015.

[20] G. Hao and J. Yu, "Design, modelling and analysis of a completely-decoupled XY compliant parallel manipulator," *Mechanism and Machine Theory*, vol. 102, pp. 179–195, 2016.

[21] Y. Liu and Z. Zhang, "A large range compliant nano-manipulator supporting electron beam lithography," *Journal of Mechanical Design*, vol. 144, no. 4, p. 043303, 2022.

[22] S. Awtar, A. H. Slocum, and E. Sevincer, "Characteristics of beam-based flexure modules," *Journal of Mechanisms and Robotics*, vol. 129, no. 6, pp. 625–639, 2007.

[23] J.-J. Kim, Y.-M. Choi, D. Ahn, B. Hwang, D.-G. Gweon, and J. Jeong, "A millimeter-range flexure-based nano-positioning stage using a self-guided displacement amplification mechanism," *Mechanism and Machine Theory*, vol. 50, pp. 109–120, 2012.

[24] Z. Lyu and Q. Xu, "Design of a new bio-inspired dual-axis compliant micromanipulator with millimeter strokes," *IEEE Transactions on Robotics*, vol. 39, no. 1, pp. 470–484, 2022.